IOP Publishing New J. Phys. 17 (2015) 075007 doi:10.1088/1367-2630/17/7/075007

New Journal of Physics
The open access journal at the forefront of physics

Deutsche Physikalische Gesellschaft DPG
IOP Institute of Physics

Published in partnership with: Deutsche Physikalische Gesellschaft and the Institute of Physics

OPEN ACCESS

RECEIVED
1 April 2015

REVISED
4 June 2015

ACCEPTED FOR PUBLICATION
10 June 2015

PUBLISHED
9 July 2015

PAPER

Quantum Otto cycle with inner friction: finite-time and disorder effects

A Alecce[1], F Galve[2], N Lo Gullo[1,3], L Dell'Anna[1,3], F Plastina[4,5] and R Zambrini[2]

[1] Dipartimento di Fisica ed Astronomia G. Galilei, Università di Padova, Via Marzolo 8 Padova (PD) Italy
[2] IFISC (UIB-CSIC), Instituto de Física Interdisciplinar y Sistemas Complejos, UIB Campus, E-07122 Palma de Mallorca, Spain
[3] CNISM, Sezione di Padova, Italy
[4] Dip. Fisica, Università della Calabria, 87036 Arcavacata di Rende (CS), Italy
[5] INFN-Gruppo collegato di Cosenza, Cosenza Italy

E-mail: roberta@ifisc.uib-csic.es

Keywords: inner friction, Otto cycle, quantum thermodynamic

Abstract

The concept of inner friction, by which a quantum heat engine is unable to follow adiabatically its strokes and thus dissipates useful energy, is illustrated in an exact physical model where the working substance consists of an ensemble of misaligned spins interacting with a magnetic field and performing the Otto cycle. The effect of this static disorder under a finite-time cycle gives a new perspective of the concept of inner friction under realistic settings. We investigate the efficiency and power of this engine and relate its performance to the amount of friction from misalignment and to the temperature difference between heat baths. Finally we propose an alternative experimental implementation of the cycle where the spin is encoded in the degree of polarization of photons.

1. Introduction

The recent boosting interest in the study of the quantum counterpart of classical well-known heat engines such as the Otto, Carnot, Stirling, and Szilard ones [1–8], has been motivated both by the need of a fundamental understanding of the limits imposed by quantum mechanics on the thermodynamic performances of small devices (in terms of both efficiency and power output) and by the growing experimental ability to control various types of quantum systems with a high degree of accuracy. There have been, indeed, many proposals aimed at implementing thermodynamic transformations and cycles with many different quantum working substances, ranging from trapped ions to magnetic materials [9], with the prospect of building quantum heat engines, exploring the abilities and limitations of quantum machines in converting heat into work, and, on more general ground, building a self-contained description of thermodynamics in the quantum regime. As a specific example, an interesting proposal in this respect has been made for implementing a nanoheat engine with a single trapped ion performing a quantum Otto cycle (QOC) [10]. Besides its specific applications, this is an important example, as the QOC constitutes a useful test ground to study irreversibility in the quantum realm.

Indeed, the cycle consists of two isochoric thermalization branches (with a fixed system Hamiltonian) and two isentropic branches, in which the system is detached from the thermal baths and its evolution is generated by a parametric time-dependent Hamiltonian. Every practical realization of these latter transformations has to face the general problem of understanding and describing the (unwanted) irreversible entropy production, which can occur in non-ideal, finite-time quantum parametric processes. This general problem has been variously analyzed through the use of fluctuation relations [11, 12] and has attracted a lot of attention in recent years [13, 14].

In this paper, we explicitly address the study of the Otto cycle by focusing on the finite-time case and discussing the implications of finite-time transformations as opposed to ideal, infinitely lasting ones. In this respect, in a series of papers, Kosloff and Feldmann [15–17] introduced the concept of intrinsic/inner friction, whereby the engine is never able to accomplish a frictionless adiabatic transformation and thus loses power. This concept has been extended and applied to various contexts [12, 18, 19].

Inner friction is a fully quantum phenomenon, whose consequences are similar to those of the mechanical friction occurring when displacing a piston in compressing/expanding a gas in a classical thermodynamic setting. Its origin, however, is completely different: when the external control Hamiltonian does not commute with the internal one, the states of the working fluid cannot follow the instantaneous energy levels, leading to additional energy stored in the working medium. Inner friction is thus associated to diabatic transitions, i.e., changes of populations which occur during the time-dependent adiabatic (here referring to a closed system) strokes if they are performed at finite speed.

So far inner friction occurring in specific cycles and transformations has been analyzed by adopting phenomenodlogical and physically motivated assumptions about the explicit time dependence of the population changes (e.g., in [15], a friction coefficient is introduced, giving rise to a constant dissipated power). Our treatment, instead, does not rely on any ad hoc assumption, but rather on the exact dynamics of the working substance. This is important because it has been shown [12] that inner friction is not only an indicator of irreversibility of a quantum process, but also a quantitative measure of its amount. It is therefore crucial to identify and highlight its role in the efficiency reduction of finite-time cycles by analyzing the full quantum dynamics that produces it.

In particular, we will explore the quantum friction arising from disorder within the sample playing the role of a working substance. We will consider an ensemble of qubits in a setting in which their Hamiltonian parameters are not homogeneous and connect the presence of these *static errors* to the appearance of friction and losses during the implementation of the Otto cycle. Explicitly, we provide a *quantitative* analysis of the amount of losses due to the inner friction as a function of the degree of disorder.

Indeed, the performance of the heat machine is negatively affected by inner friction, and the cycle's outputs, such as extracted work, power, and efficiency, are gradually suppressed as disorder and friction increase.

The remainder of the paper is organized as follows. In sections 2.1 and 2.2 we introduce and review the concept of inner friction by focusing on the particular case of a spin system in the presence of misalignments and disorder, which will then be of interest for the rest of the present paper. In section 2.3 we introduce the QOC and its constituent transformations, specifying the assumptions about the model we use to describe the working substance. In section 3 we present and discuss our main results, while in section 4 we propose a feasible experimental implementation of the QOC in order to test our findings. Finally, section 5 is devoted to some concluding remarks and to a discussion of possible future developments.

2. Model and methodology

In this section we introduce the model and give a possible explanation of the origin of inner friction. We then introduce the QOC and the figures of merit through which the cycle will be characterized.

2.1. Misalignment and disordered samples

In order to understand what we mean by losses and friction in a closed quantum system, and in particular in the case of one qubit, let us focus on the dynamics generated by a Hamiltonian of the form:

$$H(\lambda(t)) = \frac{\omega_0}{2}\sigma_z + \lambda(t)(\cos\theta\sigma_z + \sin\theta\sigma_x). \tag{1}$$

The analysis reported here applies to the general case of qubit dynamics (1), and in the following we will consider the case of a spin interacting with a magnetic field (sections 2 and 3) as well as of a qubit encoded in photon polarization (optical implementation in section 4).

An adiabatic transformation is obtained by the unitary time evolution generated by the Hamiltonian (1), with a linear driving of the external field at a fixed rate $\lambda(t) = \alpha\omega_0 t/2$, which we allow to be misaligned by an angle θ with respect to the static field ω_0. The misalignment affects the energy spacing as well as the eigenstates and the populations.

We assume that at $t = 0$ the qubit in a thermal state is at inverse temperature β. For a very slow driving, ideally taking an infinite-time to complete the transformation in the quantum adiabatic regime, the qubit populations would remain unchanged while the the energy spacing increases/decreases, and the system remains in a thermal state with a lower/higher temperature. The same occurs in the absence of misalignment, $\theta = 0$ in equation (1), as in this simple scenario, where the adiabatic transformation

$$H = \omega(t)\sigma_z, \quad \text{with } \omega(t) = \frac{\omega_0}{2} + \lambda(t) \tag{2}$$

reduces to a compression/expansion of the energy spacing of the qubit, thus preserving the initial thermal populations even in the presence of fast driving.

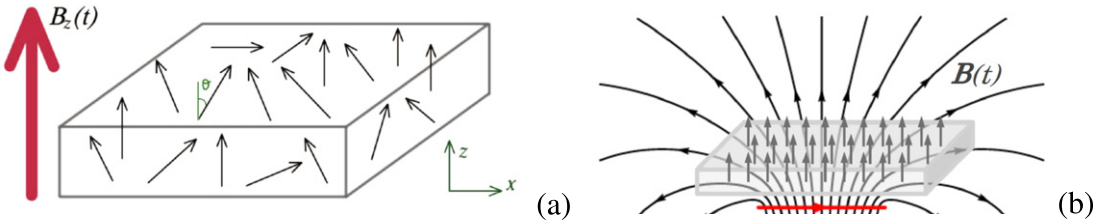

Figure 1. Misalignment effects of a sample of spins interacting with an external field due to (a) disorder within the sample or (b) lack of uniformity of the magnetic field (e.g., because of the finite length of the coil).

Interesting dynamical and thermodynamical implications arise, instead, when considering deviations from the limit of perfect alignment ($\theta \neq 0$). This is the case that we are going to explore in this work in order to characterize inner friction and its effects on the efficiency of quantum thermal machines, resulting from the simultaneous presence of the static field ω_0 and of the misaligned time-dependent part $\lambda(t)$. Our aim it to apply this analysis to an ensemble of (independent) spins, considering some degree of disorder and looking at average effects across the sample. In particular, this can correspond to different situations, as represented in figure 1. A condensed system on a lattice, with embedded magnetic dipoles having disordered orientations, can be modelled by randomly oriented spins with tilting angles θ_i ($i = 1, 2, \ldots$) with respect to the direction of a uniform external field. We assume that the distribution of the spin orientations in the sample is given by a function $G(\theta)$. Alternatively, all sample dipoles could be perfectly aligned in an ordered configuration, but the inner friction could be due to inhomogeneity of the external fields in space (figure 1(b)). The field orientation across the sample would be given, in this case, again by the function $G(\theta)$.

2.2. Inner friction and irreversibility

In order to have a simple physical picture for the behavior of our quantum machine, let us first consider the simpler case of a driven quantum two-level system undergoing the unitary dynamics generated by a parametric, time-dependent Hamiltonian $H[\lambda(t)]$. If the parameter $\lambda(t)$ changes slowly enough (in the sense of the quantum adiabatic theorem [20, 21]), the system evolves without its energy population ever changing at all, even if the instantaneous energy eigenvalues and eigenstates do change in time. If the system has been prepared in equilibrium with a thermal bath, which is then removed, such an ideal adiabatic parameter change keeps the system in an equilibrium state at every stage. In particular, if the parameter λ gets back to its initial value after some time, the final result is that the system is brought back to its initial state. On the other hand, if the cycle is performed in finite-time, the final state of the system will differ from the equilibrium state it started in, because a non-adiabatic transition has taken place [22]. The difference between the two states, if properly quantified, can be regarded as a measure of the deviation from an ideal adiabatic transformation. The quantum non-adiabaticity has the same effects as friction has in a classical context: an extra energy is needed to complete the process (indeed, the work done in the ideal adiabatic is always smaller than the one performed in finite-time; see [12, 21]), which is then dissipated if the system equilibrates at the end of the process.

With this picture in mind, let us now address the dynamics generated by Hamiltonian (1) on an initial thermal state given by $\rho_0 = \exp\{-\beta H(\lambda(0))\}/\mathrm{Tr}[\exp\{-\beta H(\lambda(0))\}]$, where β is the inverse temperature in units of the Boltzmann constant. By changing $\lambda(t)$ very slowly from $\lambda(0)$ at $t = 0$ up to $\lambda(t_f) = \lambda^\star$ at $t = t_f$ and then going back from $\lambda^\star$ to $\lambda(0)$, the system will be brought back into its initial state. To discuss what happens in the general case, namely, when these changes are performed at finite rates, we consider the following protocols:

$$\begin{aligned} \rho_0 &\xrightarrow{U_F(0,t_F)} \rho_1 \\ \rho_2 &\xleftarrow[U_B(0,t_B)]{} \rho_1 \end{aligned} \tag{3}$$

The forward protocol, defined by the unitary operator $U_F(0, t_F) = \mathcal{T} e^{-i\int_0^{t_F} H(\lambda_F(\tau))d\tau}$ ($\mathcal{T}$ being the time ordering operator), is generated by the Hamiltonian in equation (1), such that $\lambda_F(t) = \alpha_F \omega_0 t/2$. It takes the initial density matrix ρ_0 to $\rho_1 = U_F(0, t_F)\rho_0 U_F^\dagger(0, t_F)$. The backward protocol $U_B(0, t_B) = \mathcal{T} e^{-i\int_0^{t_B} H(\lambda_B(\tau))d\tau}$ is again generated by the Hamiltonian in equation (1), where now $\lambda_B(t) = \lambda_F(t_F) - \alpha_B \omega_0 t/2$ with the condition that $\lambda_B(t_B) = \lambda_F(0)$. This consists just in ramping up and down the field $\lambda(t)$ with different rates α_F and α_B, respectively.

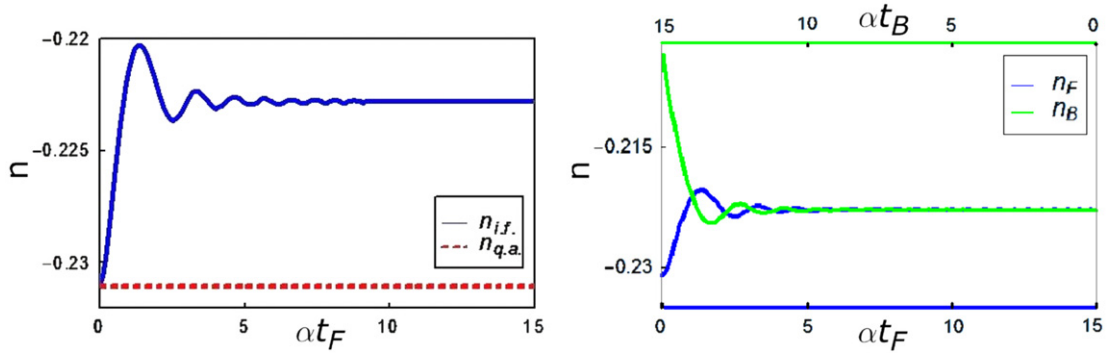

Figure 2. The left panel shows the time dependence of the polarization $n(t)$ for a finite-time adiabatic transformation (solid blue line) compared with the case of an ideal quantum adiabatic one (dashed red line). We used $\alpha_F = 10^{-4}\omega_0$. In the right panel, we compare the forward evolution (lower time axis from left to right) with the backward one (upper time axis from right to left) by displaying the time-dependent polarization in both processes. The parameters used are $\alpha_F t_F = \alpha_B t_B = 15$ and $\alpha_F = \alpha_B = \omega_0$. In both figures $\theta = \pi/5$.

In order to characterize the above protocol, we first look at the time-dependent polarization, defined as $n(t) = \mathrm{Tr}[\rho(t)H(t)]/\omega(t)$, where $\omega(t)$ is the energy level spacing at time t for both the forward and backward protocols. The result is shown in figure 2(a), where we notice that finite-time evolution introduces deviations with respect to the quantum adiabatic case, as expected. Moreover, as it can be seen in figure 2(b), by applying the forward and backward protocols defined above, the system does not get back to its initial state, but reaches a different polarization (green line) at the end of the protocol. This already gives a quantitative indication that finite-time control leads to an irreversible behavior. Here, we use the word 'irreversibility' in the thermodynamic sense: because of the occurrence of non-adiabatic transitions, the system is driven out of the manifold of equilibrium states, and application of the same protocol in reverse does not bring it back to the initial state.

A more precise way of quantifying the irreversibility of such a transformation is through the distance of the final state from the initial one, expressed in terms of the relative entropy $D(\rho_2||\rho_0)$, where $\rho_2 = U_B(0,\ t_B)\rho_1 U_B^{\dagger}(0,\ t_B)$. As shown in [12], this quantity has a well-defined thermodynamical interpretation, as it precisely gives the non-adiabatic part of the work performed on the system by the driving agent, i.e., the inner friction.

Indeed, for an adiabatic transformation, the quantum relative entropy between the actual final state and the ideal thermal equilibrium one is proportional to the difference between the work done on the system during the parametric change and the same quantity taken in the infinitely slow limit. This is precisely the definition of the inner friction, hereafter called W_{fric} [12]. Furthermore, the same quantity is linked to the generation of extra heat, that is to say, to the irreversible production of 'waste energy.' This extra energy is exactly the energy that needs to be dissipated if, at the end of the protocol, we were to thermalize the system to the initial temperature. Specifically, the following relations hold:

$$-\beta Q(\rho_2 \to \rho_0) = \beta W_{fric} = D\left(\rho_2 \middle|\middle| \rho_0\right) \tag{4}$$

where $Q(\rho_2 \to \rho_0)$ is the heat the system takes to thermalize at the initial inverse temperature β. This is what we shall refer to as inner friction in the following.

The inner friction for the time evolution described above is reported in figure 3, where we can clearly see that when both transformations are either very slow (quantum adiabatic case) or very fast ('diabatic' or sudden case); at the end of the protocol the system is found to be in (or very close to) its initial state. For finite-time transformations, however, the system does not get back to its initial state. From a dynamical point of view, this is not surprising; however, if interpreted from a thermodynamical perspective, this fact suggests that transformations done in finite-time are, in general, irreversible ones.

2.3. Model for the quantum Otto cycle (time scale assumptions)

The Otto cycle is the simplest cycle for our purposes, as it allows for a clear separation between dissipative steps (thermalization processes, in contact with a thermal bath) from non-dissipative ones (in which work is done or extracted), as opposed, for instance, to the Carnot cycle, which contains two isotherms in which one has to perform (extract) work while the system is attached to a thermal bath. This separation will be very useful in order to identify finite-time effects on the single adiabatic transformations and thus on the total cycle.

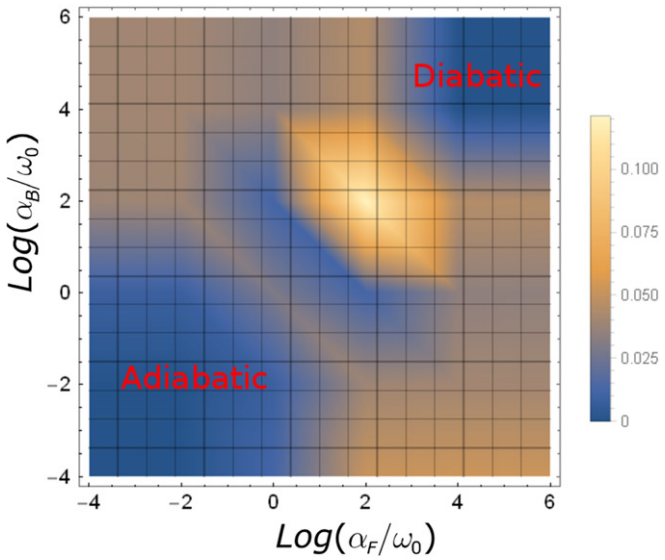

Figure 3. The quantum relative entropy between the state at the end of the backward step and the initial thermal state ρ_0. Notice that inner friction is very close to zero both for $\alpha_{F,B} \to 0$ and $\alpha_{F,B} \to \infty$. The inverse temperature characterizing the initial state is taken to be equal to the energy spacing ω_0. Here $\theta = \pi/5$ and $\alpha_F t_F = \alpha_B t_B = 15$.

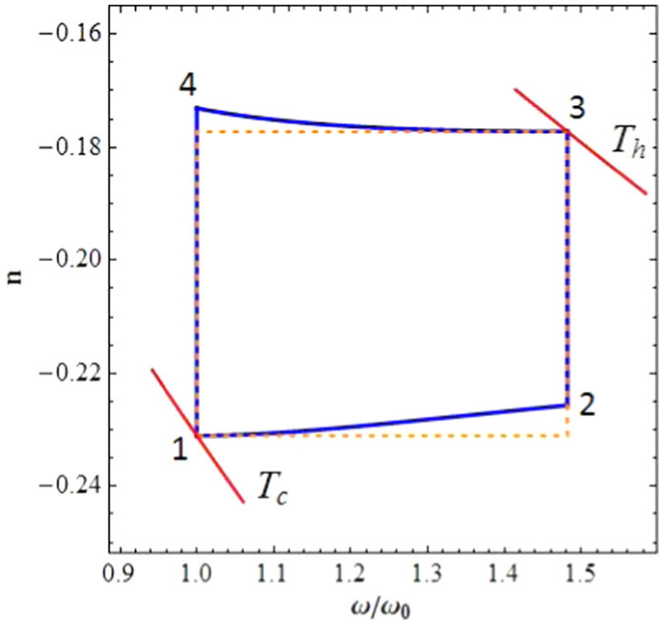

Figure 4. Representation of the Otto cycle in a parameter space in which the horizontal axis gives the instantaneous energy spacing between the eigenstates of the Hamiltonian (1), while the vertical axis gives the polarization. The solid blue line is an example of a finite-time Otto cycle with parameters: $\theta = \frac{\pi}{5}$, $\alpha t = \omega_0 t = 0.5513$, $\beta_c = \omega_0^{-1}$ and $\beta_h = \beta_c/2$. The dashed yellow line corresponds to an ideal (infinite-time) Otto cycle. The two red lines are the isotherms in this plane. They include the two (very fast) branches in which the system equilibrates in contact with baths at inverse temperatures β_c and β_h, respectively.

The quantum version of the Otto cycle is the composition of two adiabatic transformations, in which the systems evolves unitarily, and two isochoric branches corresponding to thermalization in contact with a hot (and, respectively, a cold) heat bath at temperature β_h^{-1} (β_c^{-1}).

In the next subsections we better specify the assumptions we employ to describe the different branches of the QOC and the physical quantities we investigate to characterize it. The ideal Otto cycle is represented by the dashed (yellow) rectangle in figure 4. The blue line, instead, describes a finite-time cycle in which the endpoints of the adiabatic strokes are moved towards larger values of n (which just means that there is more population than expected in the excited states) because of the presence of inner friction.

2.3.1. Adiabatic transformation

As already mentioned above, the adiabatic transformations can be described by the unitary operator generated by the Hamiltonian in equation (1). For simplicity, in the following we will consider the case where the two adiabatic branches ($1 \rightarrow 2$ and $3 \rightarrow 4$) last equally long, namely, $t_F = t_B = \tau_{ad}$, and have the same rate of change for the field $\alpha_F = \alpha_B$.

2.3.2. Isochoric transformations

For the isochoric transformations, we assume perfect thermalization at the given temperatures β_h^{-1}, β_c^{-1} (hot and cold, respectively). To study the relation between inner friction and the finite-time of the adiabatic branches, we will assume that perfect thermalization is achieved very quickly with respect to all other time scales and also that the isochoric branch will be assigned with a fixed short-time duration (to be eventually neglected) with respect to adiabatic ones, but long with respect to thermalization time of the system:

$$\tau_{therm} \ll \tau_{iso} \ll \tau_{ad} \tag{5}$$

where τ_{therm}, τ_{iso}, and τ_{ad} are the typical time scales for the thermalization process, isochoric and adiabatic transformations, respectively.

2.4. Figures of merit

In order to characterize the QOC, we will look at the extractable work, W_{ex}, at the power $\mathcal{P}$, at the efficiency η, and at their averages over disorder.

To properly define these quantities, let us start by defining the work done on an adiabatic branch as:

$$W = \mathrm{Tr}\Big[H_f \rho_f\Big] - \mathrm{Tr}\Big[H_i \rho_i\Big] \tag{6}$$

where H_i (H_f) and ρ_i (ρ_f) are the Hamiltonian and the density matrix of the system at the beginning (end) of each transformation. In particular, both adiabatic transformations start with a Gibbs-like state, since we assume perfect thermalization to occur at the end of each isochore. In the adiabatic transformations, the work defined in equation (6) does coincide with the first moment of the work distribution for closed but non-autonomous systems [25]. On the other hand, such a work distribution allows to define a fluctuation relation, and thus its moments have a clear thermodynamical meaning.

In the isochoric branches, we have that the initial and final Hamiltonians are the same, and the final state ρ_f is thermal and thus diagonal in the energy eigenbasis. The amount of energy exchanged between the reservoir and the system in each isochoric transformation is given by:

$$Q_{iso} = \epsilon_1\Big(p_1^{(f)} - p_1^{(i)}\Big) + \epsilon_0\Big(p_0^{(f)} - p_0^{(i)}\Big) \equiv \omega\Big(p_0^{(i)} - p_0^{(f)}\Big). \tag{7}$$

Thus, the energy absorbed from the bath equals the energy spacing $\omega = \epsilon_1 - \epsilon_0$ times the change in the population of the lowest energy state. (We denoted the ground and excited state populations as p_0 and p_1, respectively.)

Since the change of the total internal energy along the cycle vanishes, the total work done on the system is given by $W_{tot} = -(Q_h + Q_c)$, where Q_h (Q_c) is the amount of energy exchanged with the reservoir at inverse temperature β_h (β_c), given by equation (7) for the isochores $2 \rightarrow 3$ ($4 \rightarrow 1$). The first quantity we will use to characterize the cycle is the extractable work $W_{ex} = -W_{tot} = (Q_h + Q_c)$ given by the relation:

$$W_{ex} = \Big(\omega_2\Big(p_0^{(2)} - p_0^{(3)}\Big) + \omega_1\Big(p_0^{(4)} - p_0^{(1)}\Big)\Big), \tag{8}$$

where $\omega_k = (\epsilon_1^{(k)} - \epsilon_0^{(k)})$ is the energy level spacing of the Hamiltonian at point $k = 1, 2$ in the ω-n diagram of figure 4.

For the QOC, and by means of the definition of n, we can then write the following condition

$$\omega_1(n_{(1)} - n_{(4)}) < \omega_2(n_{(2)} - n_{(3)}), \tag{9}$$

ensuring that the work extracted is strictly positive, and we are actually using the engine to perform the work. This is in agreement with the Carnot theorem, as shown in [15], and for ideal quantum adiabatic branches (i.e., infinitely slow transformations) it reduces to $\beta_h/\beta_c > \omega_1/\omega_2$, where $\omega_{1,2}$ are the energy spacings at the end of the *quantum adiabatic* branches [23]. Notice that, in this quantum adiabatic limit, a breakdown of the positive work condition coincides with the saturation of the Carnot inequality.

Let us now define the power and the efficiency of a cycle on a single qubit as:

$$\mathcal{P}\Big(\tau_{ad}, \theta, \beta_h/\beta_c\Big) = \frac{W_{ex}}{t_F + t_B + \tau_{iso}} = \frac{W_{ex}}{2\tau_{ad} + \tau_{iso}}, \tag{10}$$

$$\eta\left(\tau_{ad},\,\theta,\,\beta_h/\beta_c\right) = \frac{W_{ex}}{Q_h} = 1 + \frac{Q_c}{Q_h} \tag{11}$$

where we have made explicit the dependence upon the angle θ in both $\mathcal{P}$ and η, and we explicitly included τ_{iso} in the above definitions, despite the assumption that it is small compared to the characteristic timescale of the cycle, just to avoid that $\mathcal{P}$ is ill-defined in the formal limit $\tau_{ad} \to 0$.

In addressing the disordered case we average all quantities over θ, assuming it to have a Gaussian distribution $G_\sigma(\theta)$ with zero mean and variance σ^2. The averaged extractable work, power, and efficiency are thus given by:

$$\overline{W}_{ex}\left(\tau_{ad},\,\beta_h/\beta_c,\,\sigma\right) = \int_0^\pi G_\sigma(\theta)\, W_{ex}\left(\tau_{ad},\,\theta,\,\beta_h/\beta_c\right) \mathrm{d}\theta \tag{12}$$

$$\overline{\mathcal{P}}\left(\tau_{ad},\,\beta_h/\beta_c,\,\sigma\right) = \int_0^\pi G_\sigma(\theta)\, \mathcal{P}\left(\tau_{ad},\,\theta,\,\beta_h/\beta_c\right) \mathrm{d}\theta \tag{13}$$

$$\overline{\eta}\left(\tau_{ad},\,\beta_h/\beta_c,\,\sigma\right) = \int_0^\pi G_\sigma(\theta)\, \eta\left(\tau_{ad},\,\theta,\,\beta_h/\beta_c\right) \mathrm{d}\theta. \tag{14}$$

3. Results and discussion

In this section we characterize the QOC by looking at the extractable work W_{ex}, its power $\mathcal{P}$, and its efficiency η, paying particular attention to the role of the inner friction in limiting the performances of such a heat engine. In the first subsection we will look at these figures of merit for different sets of parameters of our model-system. In the second one, we study the behavior of the efficiency at maximum power, $\eta(\mathcal{P}_{MAX})$.

3.1. Extractable work, power, and efficiency

In what follows we will study the performance of the QOC in various cases of equal rates for both of the adiabatic branches. In figures 5(a), (c) and (e) we plot W_{ex}, $\mathcal{P}$, and η, as functions of the total time of the cycle t_{tot} for different values of the misalignment angle θ at a fixed value of the ratio between the temperatures of the hot and cold reservoirs $\beta_h/\beta_c = 0.5$. It can be seen that the extractable work becomes negative if the t_{tot} exceeds a maximum time $t_M(\theta)$, which is a function of the misalignment θ. This means that if the cycle lasts too long, we are actually doing work on the system. Moreover there exists a critical value of θ such that the extractable work is negative for any value of t_{tot}. Under these conditions, the cycle is not a heat engine but rather a refrigerator, which uses external work to cool the cold reservoir. An analogous behavior is shown by power and efficiency.

In figures 5(b), (d) and (f), we show the dependence of W_{ex}, $\mathcal{P}$, and η on the total time of the cycle for a fixed misalignment angle $\theta = \pi/5$ and for different values of the ratio β_h/β_c. We can see that as the ratio increases, the extractable work increases too. This is something which is expected; nevertheless, we can clearly see that the finiteness in the time of the cycle introduces again negative works for $t_{tot} > t_M(\beta_h/\beta_c)$. This is again due to the generation of inner friction, which comes along with the finite-time condition.

Inner friction is explicitly shown in figure 6, where the sum of the friction produced in the two adiabatic strokes is shown as a function of the total cycle time for various misalignment angles θ. As discussed above, the case $\theta = 0$ is very special, as no friction is generated, whatever rate of variation is considered for the driving field $\lambda(t)$. On the other hand, W_{fric} increases with increasing the tilting angle θ and decreases with decreasing the driving rate α. The behavior of W_{fric} should be compared to that of W_{ex} shown in figure 5: the more friction is present, the less work can be extracted from the engine.

So far we have considered QOCs with given values of the misalignment angle θ. We now consider the effect of disorder and assume that θ is a Gaussian random variable with mean value $\overline{\theta} = 0$ and variance σ^2. In figures 7(a), (c), and (e) we show the behavior of extractable work, power, and efficiency for different values of the variance and given temperature ratio ($\beta_h/\beta_c = 0.5$). We can see that at a given total time t_{tot}, the best performance is always obtained with sharper distributions (smaller σ). Thus, if the disorder of the system grows, the capability of the latter of providing work and of doing it in a more efficient way decreases. Again we mention the fact that there exists a maximum total time t_M above which the QOC is not a heat engine anymore. We also notice that even a small disorder has quite a dramatic effect in reducing the efficiency for long enough times (upper curve in figure 7(e)).

In figures 7(b), (d), and (f) we plotted the behavior of the same quantities for different values of the ratio β_h/β_c at a given variance $\sigma^2 = 0.1$. Again, all of the quantities increase as the difference in temperatures increases.

We plotted all of the quantities as a function of the total cycle time t_{tot} because, from an operational point of view, this is the quantity one can control once the working substance is prepared and the stage is set for the thermal machine to operate. However, it has to be mentioned that some care should be paid when comparing the values of the efficiency at different operating times. Indeed, since ω varies with time, each different t_{tot} gives rise to a different value of the final frequency (called ω_2, above) at which the isochoric $2 \to 3$ takes place; see

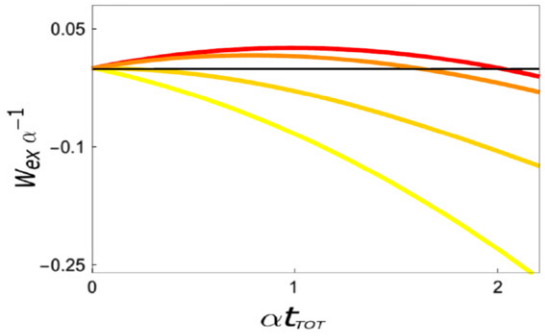

(a) Extractable work (W_{ex}) vs. αt_{tot} for different values of θ

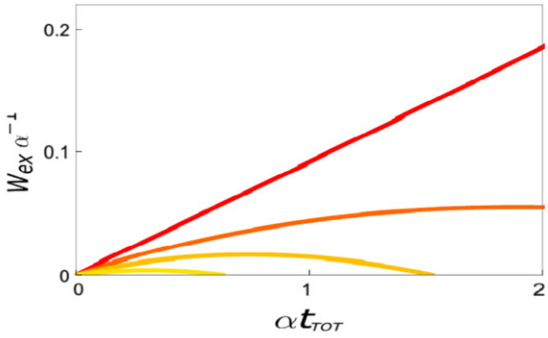

(b) Extractable work (W_{ex}) vs. αt_{tot} for various β_h/β_c

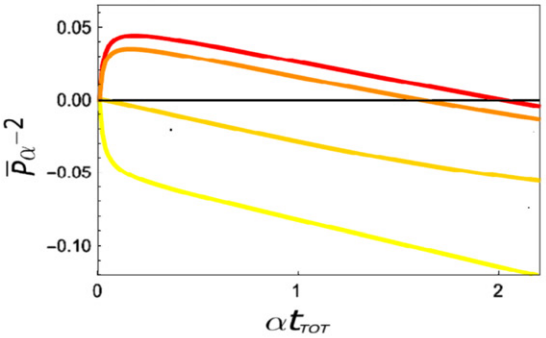

(c) Power ($\mathcal{P}$) vs. αt_{tot} for various of θ

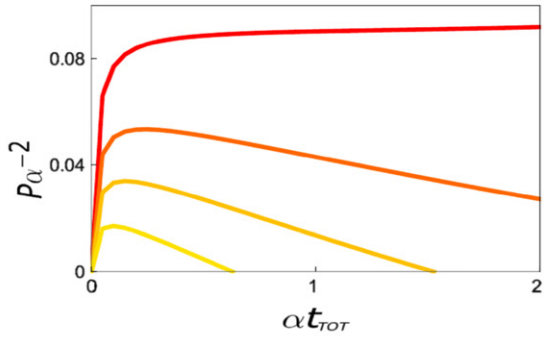

(d) Power ($\mathcal{P}$) vs. αt_{tot} for various of β_h/β_c

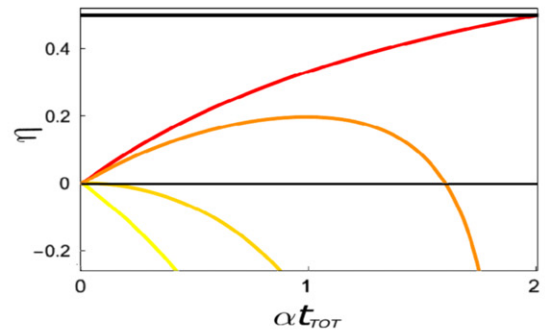

(e) Efficiency (η) vs. αt_{tot} for various θ

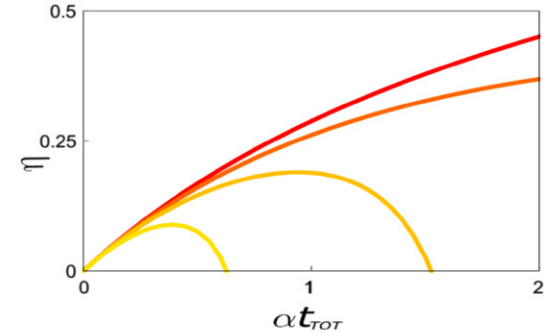

(f) Efficiency (η) vs. αt_{tot} for various β_h/β_c

Figure 5. Extractable work, power, and efficiency as functions of αt_{tot}. In figures 5(a), (c), and (e) we fix the temperature ratio $\beta_h/\beta_c = 0.5$ and vary the misalignment θ, starting from $\theta = 0$ for the highest (red) plot, then considering $\theta = \pi/5,\ \pi/2$ and finally $\theta = \pi$ for the lowest (yellow) curve. On the other side, in 5(b), (d), and (f) we fix the misalignment to $\theta = \pi/5$ and vary β_h/β_c, which, again going from the top-most red plot down to the yellow curve, takes the values $\beta_h/\beta_c = 0.01,\ 0.31,\ 0.51,\ 0.71$.

figure 4. The ideal cycle with infinitely slow adiabatic branches, corresponding for us also to the absence of misalignment ($\theta = 0$) and shown for comparison in each plot in figures 5 and 6, has efficiency $\eta_{ideal} = 1 - \frac{\omega_1}{\omega_2}$. The dependence of η_{ideal} on ω_2 implies that the efficiency η should be compared with a different η_{ideal} at each different t_{tot}. To avoid any confusion in this respect, and to better display the role of finite-time induced friction in the machine performance, we show this comparison in figure 8, where the ratio η/η_{ideal} is displayed as a function of the operating time. Once the efficiency is renormalized in this way, its residual dependence on t_{tot} can be fully ascribed to the presence of inner friction.

3.2. Efficiency at maximum power

Let us now consider the relation between η and $\mathcal{P}$ (see figure 9) and then extract the value of the efficiency at maximum power $\eta\,(\mathcal{P}_{MAX})$. Two sets of these data are reported in tables 1 and 2. They refer to averaged power

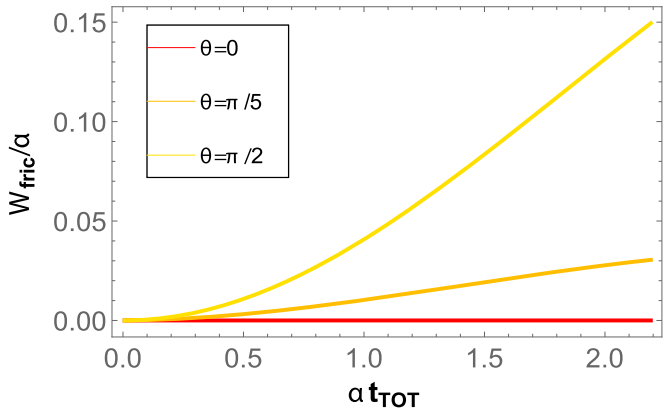

Figure 6. Inner friction accumulated in the cycle as a function of the total operation time for different misalignments θ, at $\beta_h/\beta_c = 0.5$.

and efficiency considering in the first case various temperature ratios at a fixed width, and the other way round for the second case. The effects of disorder and temperature difference continue to stand: our analysis provides larger values of (averaged) power and (averaged) efficiency at maximum power for smaller and smaller σ and for larger and larger β_h/β_c, with the following one-sentence summary: we obtain considerably larger values of $\eta(\mathcal{P}_{MAX})$ when the temperature ratio is large and for very picked misalignment G distributions, that is, when the inner friction is smaller.

4. Experimental implementation with an optical setup

In this section we propose one possible experimental set-up by means of which it is possible to realize the Otto cycle discussed so far and test our findings. The Otto cycle is made up of two different types of branches, namely, adiabatic and isochoric transformation. Thus the proposed set-up has to be able to implement both of them.

The physical system we have in mind is an optical one, and, in particular, we propose to encode the qubit into the polarization degree of freedom of a single photon. In the following we address the implementation of the two types of branches separately, stressing the key points for both of them.

4.1. Implementation of the adiabatic transformation

The adiabatic branch in the Otto cycle is achieved by means of a time-dependent effective magnetic field, and its time evolution is given by the unitary operator:

$$\hat{U}(t) = T\mathrm{e}^{-\mathrm{i}\int_0^t d\tau\ \vec{B}(\tau)\cdot\vec{\sigma}} \tag{15}$$

For a fixed $t = t^\star$ the above operator can be written as a rotation in the Hilbert space of the qubit using the Euler decomposition as:

$$\hat{U}(t^\star) = \mathrm{e}^{-\mathrm{i}\frac{\psi^*}{2}\sigma_z}\mathrm{e}^{-\mathrm{i}\frac{\theta^*}{2}\sigma_x}\mathrm{e}^{-\mathrm{i}\frac{\phi^*}{2}\sigma_z}. \tag{16}$$

This expression is helpful for our purposes, because the single rotations appearing in it can be easily implemented in an optical setup as rotation of the polarization degrees of freedom of a single photon.

Therefore by encoding the qubit into the polarization degree of freedom of a photon and, in particular, by choosing the basis $\{|H\rangle, |V\rangle\}$ of horizontal and vertical polarization, we can perform the wanted rotations by means of properly chosen phase retarders.

4.2. Implementation of the isochoric transformation

The isochoric transformation requires more care. By definition it amounts to attaching the system to a thermal bath, which makes the system thermalize into a Gibbs-like state. The latter is characterized by a density matrix ρ with no coherences between different eigenstates of the Hamiltonian of the system, whereas the diagonal ones are given by the Boltzmann factors $\mathrm{e}^{-\beta\epsilon_n}/(\mathrm{e}^{-\beta\epsilon_0} + \mathrm{e}^{-\beta\epsilon_1})$, where $\beta = 1/T_c$ or $\beta = 1/T_h$ is the inverse temperature we want the state to thermalize at, and ϵ_n are the eigenenergies of the final Hamiltonian of the adiabatic transformation preceding the isochoric one we are addressing. In the case of a qubit, the thermalization process leads to a final state that is diagonal in a given basis (determined by the form of the bath-spin coupling) and whose populations are related to the temperature of the thermal bath by the relation

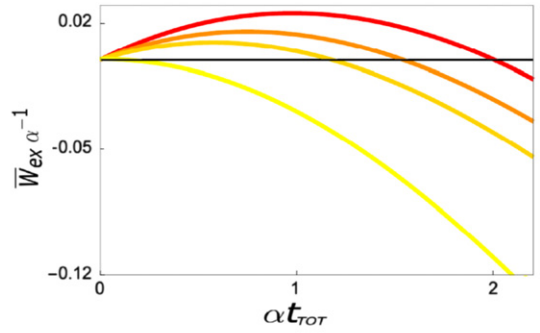

(a) Average extractable work ($\overline{W}_{ex}$) vs. αt_{tot} for various σ.

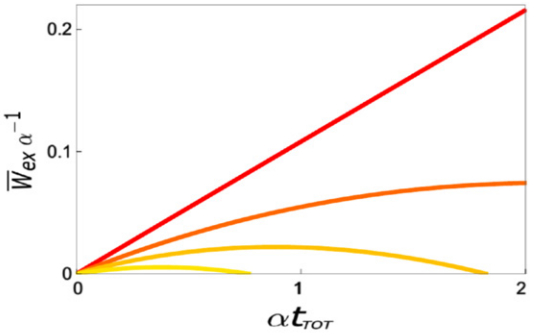

(b) Average extractable work ($\overline{W}_{ex}$) vs. αt_{tot} for various β_h/β_c.

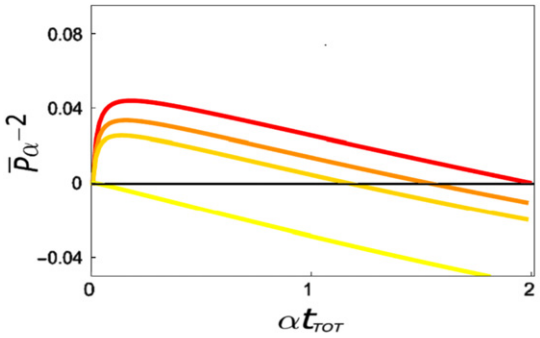

(c) Averaged power ($\overline{\mathcal{P}}$) vs. αt_{tot} for various σ.

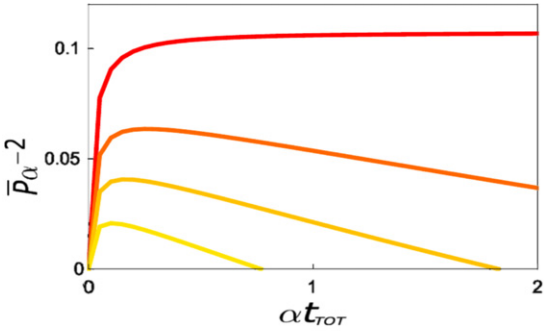

(d) Averaged power ($\overline{\mathcal{P}}$) vs. αt_{tot} for various β_h/β_c.

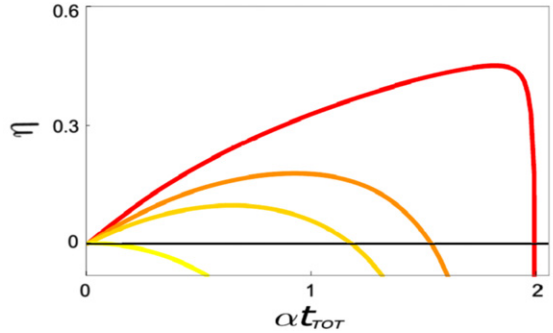

(e) Averaged efficiency ($\overline{\eta}$) vs. αt_{tot} for various σ.

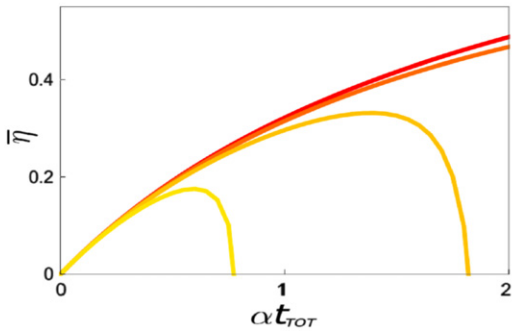

(f) Averaged efficiency ($\overline{\eta}$) vs. αt_{tot} for various β_h/β_c.

Figure 7. Averaged extractable work, power and efficiency as functions of αt_{tot}. In figure 7(a), (c), and (e), we consider a fixed value for the temperature ($\beta_h/\beta_c = 0.5$) and vary σ. Different colors refer to different Gaussian widths: the red plots correspond to $\sigma^2 = 0.01$, The orange ones to $\sigma^2 = 0.5$, light orange ones to $\sigma^2 = 1$, and, finally, the (lowest) yellow curves refer to a flat distribution. In figures 7(b), (d) and (f) we take $\sigma^2 = 0.1$, and vary β_h/β_c, which, going from the red plots to the yellow ones, takes the values $\beta_h/\beta_c = 0.01,\ 0.31,\ 0.51,\ 0.71$.

$$\beta = T^{-1} = -\frac{1}{\epsilon_1 - \epsilon_0}\log\frac{1-p_0^{(f)}}{p_0^{(f)}} \qquad \frac{1}{2} \leqslant p_0^{(f)} < 1, \tag{17}$$

where, $p_0^{(f)}$ is the population of the lowest ($n = 0$) state of the qubit after thermalization has occurred.

In order to implement an isochoric transformation we propose to exploit the experimental setup used in [24]. The idea is to exploit the spatial degrees of freedom of the photon as an effective bath for its polarization. The coupling between the two is achieved by exploiting the birefringent property of a quartz plate. The effect of the latter on a photon passing through it is to phase-shift the horizontal and vertical component of the polarization by an amount proportional to the number of photons per mode. Once the spatial part of the photon is traced out, the dynamics of the polarization turns out to be driven by the following dynamical map between an initial state ρ_i to a final state ρ_f, which describes decoherence:

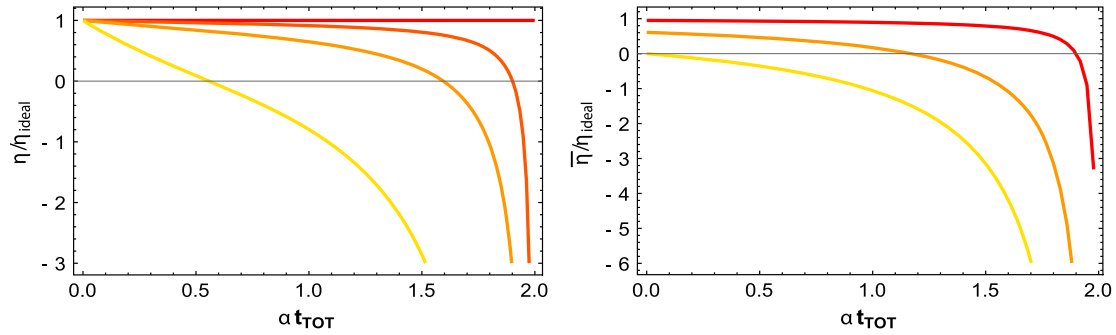

Figure 8. Left: renormalized efficiency η/η_{ideal} as a function of the total operation time for different misalignments $\theta = 0,\ \pi/10,\ \pi/5,\ 2\pi/5$, at $\beta_h/\beta_c = 0.5$. Right: averaged efficiency $\bar{\eta}$ normalized with respect to the ideal efficiency obtained at $\theta = 0$. The average is taken over Gaussian distributions with variances, $\sigma^2 = 0.1$, $\sigma^2 = 1$, and over a flat distribution, respectively. For all of the plots, we fixed the temperature ratio $\beta_h/\beta_c = 0.5$.

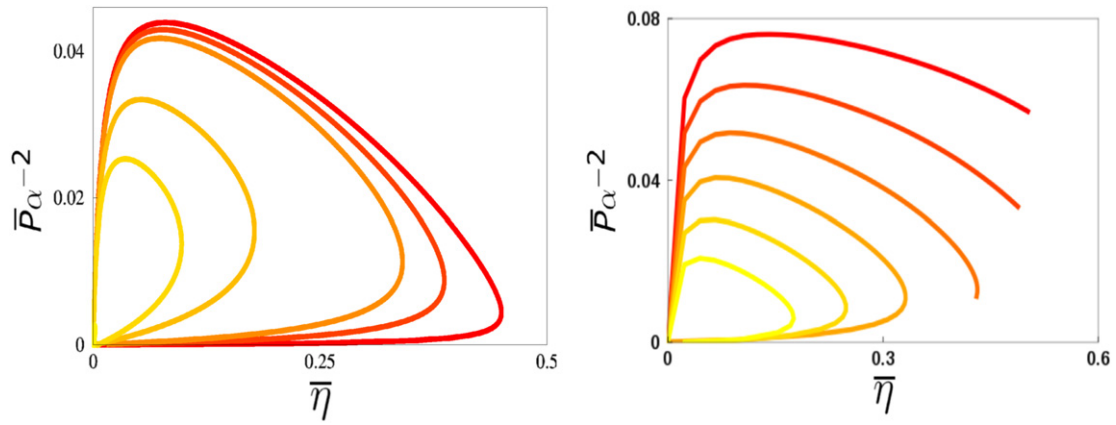

(a) $\mathcal{P}$ vs. η for various σ. (b) $\mathcal{P}$ vs.η for various β_h/β_c.

Figure 9. Relation between averaged power and efficiency, $\overline{\mathcal{P}}(t)$ and $\bar{\eta}(t)$, at the same time parameter αt_{tot}. In 9(a) we choose $\beta_h/\beta_c = 0.5$ and vary σ, which, from the outer to the inner curve takes the values $\sigma^2 = 0.01,\ 0.05,\ 0.1,\ 0.5,\ 1,\ 10$. In 9(b) we fix $\sigma^2 = 0.1$, and, starting from the outer to the inner curve, we consider the increasing temperature ratios $\beta_h/\beta_c = 0.02,\ 0.03,\ 0.04,\ 0.05,\ 0.06,\ 0.07$.

Table 1. Efficiency at maximum power at $\beta_h/\beta_c = 0.5$ and for different values of the Gaussian bell's width σ. The optimal total cycle time, αt_{tot}^{MAX}, is the one for which $\overline{\mathcal{P}}$ attains its maximum.

σ^2	αt_{tot}^{MAX}	$\overline{\mathcal{P}}_{MAX}/\alpha^2$	$\bar{\eta}\,(\overline{\mathcal{P}}_{MAX})$
0.01	0.0882	0.0439	0.0775
0.05	0.0882	0.0429	0.0758
0.1	0.0882	0.0418	0.0737
0.5	0.0771	0.0334	0.0519
1	0.0340	0.0253	0.0340
10	0.0.220	0.0027	0.0220

$$\rho_i \to \rho_f = \frac{1}{2}\Big((1+z)\rho_i + (1-z)\hat{\sigma}_z\, \rho_i\, \hat{\sigma}_z \Big), \tag{18}$$

where the parameter z can be tuned from $z = 1$ (identity map) to $z = -1$ (complete decoherence; namely, the final density matrix has vanishing off-diagonal terms). Because of our assumption of complete thermalization we will always assume $z = -1$.

We can thus exploit this mechanism in order to engineer thermalization in the following way. Let us assume that the inverse temperature of the bath we want to mimic is β. Through equation (17) we can determine the

Table 2. Efficiency at maximum power for $\sigma^2 = 0.1$ for different temperature ratios β_h/β_c. The maximum power $\overline{\mathcal{P}}_{MAX} = \overline{\mathcal{P}}\,(t_{tot}^{MAX})$ is obtained for the times αt_{tot}^{MAX} reported in the second column.

β_h	αt_{tot}^{MAX}	$\overline{\mathcal{P}}_{MAX}/\alpha^2$	$\overline{\eta}\,(\overline{\mathcal{P}}_{MAX})$
2.1	0.175	0.0761	0.1420
3.1	0.125	0.0635	0.1056
4.1	0.1	0.0517	0.0862
5.1	0.075	0.0406	0.0660
7.1	0.05	0.0208	0.0447
9.1	0.025	0.0045	0.0224

population of the lowest energy level after the system is completely thermalized. Let us write the initial state (which in turn corresponds to the final state of the adiabatic transformation preceding the isochoric one) as:

$$\rho_i = \frac{1}{2}\mathbf{1} + \left(\frac{1}{2} - p_0^{(i)}\right)\sigma_z + b_x\ \sigma_x + b_y\ \sigma_y. \tag{19}$$

Since the decoherence mapping in equation (18) has the effect of making the off-diagonal elements vanish, we first need to perform a rotation on the initial state ρ_i to turn it into a state of the form:

$$\rho_f' = \frac{1}{2}\mathbf{1} + \left(\frac{1}{2} - p_0^{(f)}\right)\sigma_z + b_x'\ \sigma_x + b_y'\ \sigma_y \tag{20}$$

where $p_0^{(f)}$ is calculated through relation in equation (17). The application equation (18) has now the effect of making $b_x' = b_y' = 0$, thus leaving us with the desired state:

$$\rho_f = \frac{1}{2}\mathbf{1} + \left(\frac{1}{2} - p_0^{(f)}\right)\sigma_z. \tag{21}$$

It is easy to see that in order to get from the state in equation (19) to the one in equation (20) we can apply a specific rotation, which has to be chosen by taking into account both states. For instance, in the case $b_y = 0$ and $p_0^{(f)} < p_0^{(i)} \leqslant 1/2$, that is, if we are 'heating' our system, the right rotation to perform is:

$$R_x\left(p_0^{(f)}, p_0^{(i)}\right) = \mathrm{e}^{-\mathrm{i}\frac{\theta_x}{2}\sigma_x} \tag{22}$$

with $\cos(\theta_x) = \left(1 - 2\,p_0^{(f)}\right)\left(1 - 2\,p_0^{(i)}\right)^{-1}$. For $b_y \neq 0$ we have solutions for $\cos(\theta_y)$ only if $-1/2 \leqslant 1/2 - p_0^{(f)} \leqslant -\left(\left(1/2 - p_0^{(i)}\right)^2 + b_y^2\right)^{1/2}$.

5. Conclusions

We have worked out an exact dynamical model with which we discussed the performance of a QOC in the presence of *inner friction*. With respect to previous approaches to the same problem, we obtained the growth of polarization in the adiabatic branches of the cycle without any ad hoc assumption, but rather by following the dynamics generated by the system Hamiltonian. In this way we have been able to deal with the irreversibility of such transformations when they are performed in a finite-time and so to better characterize the whole cycle. Finite-time evolution leads to a decrease of values of thermodynamical figures of merit for the heat engine, and we have concentrated on the extractable work, the power, and efficiency, which are partially quenched if inner friction is present.

The friction is related to the non-commutativity of the system and control Hamiltonian, due to some misalignment between the internal and control magnetic field axes. After explicitly studying its effects for a fixed (and controlled) case, we turned to the more realistic case in which such a misalignment is an unwanted side effect of the lack of control in the system, ultimately due to the presence of disorder in the sample or inhomogeneity of the magnetic field. The limiting cases are the completely ordered and disordered samples; in the first one, we obtain an ideal quantum Otto engine with efficiency given by $\eta_{ideal} = 1 - \omega_1/\omega_2$, while for the completely disordered case we showed that no positive work can be extracted from the system, which cannot behave as a heat engine at all. In the more general case of a finite-width Gaussian distribution of tilting angles θ, describing a given degree of disorder as quantified by its variance, we obtained a quantitative description of the efficiency reduction due to the disorder-induced inner friction.

Finally, we proposed an optical experimental implementation of such an Otto cycle using the effective polarization qubit of a photon, whose thermalization can be obtained by the coupling with the spatial degree of freedom in a birefringent crystal.

Acknowledgments

We acknowledge funding from FIRB 2012 RBFR12NLNA, EU, MICINN, CSIC, FEDER funding under Grants FIS2011-23526 (TIQS), FIS2014-60343-P (NOMAQ), postdoctoral JAE program (ESF), FET-proactive project QuProCS and COST Action MP1209, and the UIB for Invited Professors program.

References

[1] Quan H T, Liu Yu-xi, Sun C P and Nori F 2007 *Phys. Rev.* E **76** 031105
[2] Thomas G and Johal R S 2011 *Phys. Rev.* E **83** 031135
[3] Huang X L, Liu Y, Huang Z and Niu X Y 2014 *Eur. Phys. J. Plus* **129** 4
[4] Esposito M, Kawai R, Lindenberg K and van den Broeck C 2010 *Phys. Rev.* E **81** 041106
Polettini M, Verley G and Esposito M 2010 *Phys. Rev. Lett.* **114** 050601
[5] Scully M 2010 *Phys. Rev. Lett.* **104** 207701
[6] Huang X-L, Niu X-Y, Xiu X-M and Yi X-X 2014 *Eur. Phys. J.* D **68** 32
[7] Kim S W, Sagawa T, de Liberato S and Ueda M 2011 *Phys. Rev. Lett.* **106** 070401
[8] Campisi M 2014 *J. Phys. A: Math. Theor.* **47** 245001
Campisi M, Pekola J and Fazio R 2015 *New J. Phys.* **17** 035012
[9] Azimi M, Chotorlishvili L, Mishra S K, Vekua T, Hübner W and Berakdar J 2014 *New J. Phys.* **16** 063018
[10] Abah O, Roßnagel J, Jacob G, Deffner S, Schmidt-Kaler F, Singer K and Lutz E 2014 *Phys. Rev. Lett.* **109** 203006
Roßnagel J, Abah O, Schmidt-Kaler F, Singer K and Lutz E 2014 *Phys. Rev. Lett.* **112** 030602
[11] Jarzynski C 1997 *Phys. Rev. Lett.* **78** 2690
Mukamel S 2003 *Phys. Rev. Lett.* **90** 170604
Esposito M and van den Broeck C 2010 *Phys. Rev. Lett.* **104** 090601
Deffner S and Lutz E 2010 *Phys. Rev. Lett.* **105** 170402
[12] Plastina F, Alecce A, Apollaro T J G, Falcone G, Francica G, Galve F, Lo Gullo N and Zambrini R 2014 *Phys. Rev. Lett.* **113** 260601
[13] Esposito M, Harbola U and Mukamel S 2009 *Rev. Mod. Phys.* **81** 1665
Jarzynski C 2011 *Annu. Rev. Condens. Matter Phys.* **2** 329
Campisi M, Hänggi P and Talkner P 2011 *Rev. Mod. Phys.* **83** 771
Seifert U 2012 *Rep. Prog. Phys.* **75** 126001
[14] Dorner R, Clark S R, Heaney L, Fazio R, Goold J and Vedral V 2013 *Phys. Rev. Lett.* **110** 230601
Mazzola L, de Chiara G and Paternostro M 2013 *Phys. Rev. Lett.* **110** 230602
Batalhão T B, Souza A M, Mazzola L, Auccaise R, Sarthour R S, Oliveira I S, Goold J, de Chiara G, Paternostro M and Serra R M 2014 *Phys. Rev. Lett.* **113** 140601
Campisi M, Blattmann R, Kohler S, Zueco D and Hänggi P 2013 *New J. Phys.* **15** 105028
[15] Kosloff R and Feldmann T 2000 *Phys. Rev.* E **61** 4774
[16] Kosloff R and Feldmann T 2010 *Phys. Rev.* E **82** 011134
[17] Kosloff R and Feldmann T 2002 *Phys. Rev.* E **65** 055102
Kosloff R and Feldmann T 2003 *Phys. Rev.* E **68** 016101
Kosloff R and Feldmann T 2004 *Phys. Rev.* E **70** 046110
Kosloff R and Feldmann T 2012 *Phys. Rev.* E **85** 051114
[18] Wang J, Wu Z and He J 2012 *Phys. Rev.* E **85** 041148
[19] Wang R, Wang J, He J and Ma Y 2013 *Phys. Rev.* E **87** 042119
[20] Messiah A 1970 *Quantum Mechanics* (North Holland: Amsterdam)
[21] Allahverdyan A E and Nieuwenhuizen Th M 2005 *Phys. Rev.* E **71** 046107
[22] See, e.g. Polkovnikov A 2008 *Phys. Rev. Lett.* **101** 220402
[23] Kieu T D 2004 *Phys. Rev. Lett.* **93** 140403
[24] Liu *et al* 2011 *Nat. Phys.* **7** 931
[25] Talkner P, Lutz E and Hänggi P 2007 *Phys. Rev.* E **75** 050102(R)
Roncaglia A J, Cerisola F and Paz J P 2014 *Phys. Rev. Lett.* **113** 250601